Ultrasonic Defect Characterization Using the Scattering Matrix: A Performance Comparison Study of Bayesian Inversion and Machine Learning Schemas

Long Bai, Florian Le Bourdais, Roberto Miorelli, Pierre Calmon, Alexander Velichko, Bruce Drinkwater

Ultrasonic defect characterisation using the scattering matrix: A performance comparison study of Bayesian inversion and machine learning schemas

Long Bai, Florian Le Bourdais, Roberto Miorelli, Pierre Calmon, Alexander Velichko, and Bruce W. Drinkwater

Abstract

Accurate defect characterisation is desirable in ultrasonic non-destructive evaluation as it can provide quantitative information about the defect type and geometry. For defect characterisation using ultrasonic arrays, high resolution images can provide the size and type information if a defect is relatively large. However, the performance of image-based characterisation becomes poor for small defects that are comparable to the wavelength. An alternative approach is to extract the far-field scattering coefficient matrix from the array data and use it for characterisation. Defect characterisation can be performed based on a scattering matrix database that consists of the scattering matrices of idealised defects with varying parameters. In this paper, the problem of characterising small surface-breaking notches is studied using two different approaches. The first approach is based on the introduction of a general coherent noise model, and it performs characterisation within the Bayesian framework. The second approach relies on a supervised machine learning (ML) schema based on a scattering matrix database, which is used as the training set to fit the ML model exploited for the characterisation task. It is shown that convolutional neural networks (CNNs) can achieve the best characterisation accuracy among the considered machine learning approaches and they give similar characterisation uncertainty to that of the Bayesian approach if a notch is favourably oriented. The performance of both approaches varied for unfavourably oriented notches, and the machine learning approach tends to give results with higher variance and lower biases.

I. Introduction

ULTRASONIC non-destructive testing (NDT) is often used to detect and localise defects in a safety critical structure without causing damage to the component or radiation hazards to personnel [1], [2]. Typically, an input pulse is transmitted into the material under test and the presence of material discontinuities or defects gives rise to the reflected signal. Traditional ultrasonic testing techniques use a single-element transducer to scan the region of interest within a component and detection is achieved by comparing the amplitude of the received signal with a pre-set threshold [3]. The defect size can then be determined by the 6 dB drop approach as the distance over which the amplitude of the defect signal drops by 1/2 [4]. However, this approach is most effective for relatively large crack-like defects (*i.e.*, sizes over 2 ultrasonic wavelengths) that are favorably oriented, and from which the specular signal can be measured. A comprehensive approach is needed to characterise various types of defects that can occur in practice, such as cracks, volumetric voids, porosity and inclusions.

Ultrasonic arrays provide improved focusing capabilities compared to conventional single-element transducers and are increasingly used for inspection of structural components [5]. A data acquisition scheme known as the full matrix capture (FMC) collects A-scan signals measured from all transmitter-receiver pairs of an array [6]. These A-scan data can be properly delayed and summed in post-processing and focusing is achieved at each pixel point of the imaging plane. Besides detection, advanced imaging algorithms such as the total focusing method (TFM) [6], virtual source aperture (VSA) [7], and plane-wave imaging (PWI) [8], [9] also facilitate image-based characterisation of defects. The size of surface-breaking cracks larger than 3 mm were measured with errors less than 8% by identifying the crack tips from an image [10]. For internal cracks, the size and orientation angle were shown to be measurable using a rectangular box that covers all image pixels within -6 dB from the peak value [11]. While obtaining the crack propagation path and orientation by adopting TFM, Camacho *et al.* showed that sizing by tip detection with phase coherence imaging (PCI) was more robust than the 6 dB drop approach [12]. In addition, signal and image processing techniques were developed which improve the time resolution of the measured A-scan signals [13], [14] and spatial resolution of the ultrasonic images [15], [16]. However, when the defect size is comparable to the ultrasonic

This work was supported by National Natural Science Foundation of China under grant number 52005205, European Union's Horizon 2020 Research and Innovation Programme under grant agreement number 755500, and the Engineering and Physical Sciences Research Council (UK, EPSRC) under grant number EP/L022125/1.

Long Bai is with the State Key Laboratory of Digital Manufacturing Equipment and Technology, School of Mechanical Science and Engineering, Huazhong University of Science and Technology, Wuhan 430074, China (e-mail: bailong@hust.edu.cn).

Florian Le Bourdais, Roberto Miorelli, and Pierre Calmon are with CEA, LIST, Institute CEA Saclay - Digiteo Labs, Bat. 565-PC120, F91191, Gif-sur-Yvette Cedex, France.

Alexander Velichko and Bruce W. Drinkwater are with the Department of Mechanical Engineering, University of Bristol, Queens Building, University Walk, Bristol BS8 1TR, UK.

wavelength, the defect indication becomes indistinguishable from that of a point scatterer and image-based characterisation of small defects is fundamentally challenging.

There exist two different types of approaches in literature which have the potential to size and characterise sub-wavelength defects: defect shape reconstruction through super-resolution imaging, and inversion which aims to retrieve key defect parameters based on the availability of a forward model. Super-resolution imaging algorithms such as the time-reversal multiple signal classification (TR-MUSIC) [17] and the factorisation method (FM) [18] were used to characterise simulated rough cracks [19] and were shown to be capable of achieving a resolution beyond the diffraction limit in ideal low-noise measurement scenarios. The main issue of these algorithms is their performance degradation for non-ideal defects (such as rough and inclined cracks [19]) and noisy materials [20]. A model-based inversion approach was developed for crack sizing by utilising an analytic expression relating the crack size to the array data [21]. Li *et al.* studied the crack sizing problem in immersion setups and developed flaw-sizing curves that account for the surface condition of a component including curvature, roughness, and coating [22]. A type of more general inversion procedures iteratively update the defect geometry according to the difference between the actual and predicted measurements until a satisfactory agreement is achieved [23], [24]. Metamodels (or surrogate models) can speed up the inversion process by enabling fast evaluation of the forward model [25] and are recently used as tools for propagation of uncertainties [26]. Machine learning (ML) algorithms [27] offer another possibility to address the inverse problem, in which measurements from a number of known defects are used to train a suitable classifier [28] or regressor [29], [30]. Deep learning approaches such as the convolutional neural networks (CNNs) have been applied to 2D image data, including ultrasonic plane wave images [31], scanning electron microscopy (SEM) images [32], and images taken using hand-held cameras [33], for crack detection and characterisation. A subwavelength ultrasonic beamforming approach has been developed based on a deep neural network architecture [34], and one-dimensional CNNs are employed to address the limited-sample problem with line-level labels [35]. Besides images, measurement data used for inversion can also have different forms including A-scans [36], FMC data [37] or quantities derived from raw signals such as the scattering matrix [28]. The scattering matrix is defined for a single defect and encodes all the information about the defect geometry while an FMC dataset normally contains contributions from all defects within a component. Subwavelength defects remain distinguishable in terms of the scattering matrix but image-based inversion methods often fail when the defect size is small [11]. For the above reasons, we note that the scattering matrix is more suitable for characterisation of small defects than ultrasonic images or unprocessed FMC datasets. Beside the deep learning approaches, recently other works take on inversion based on guided wave images applied to Structural Health Monitoring problems using kernel machines for regression and classification tasks [38]. It is worth to be mentioned that comparisons between regression tasks based on kernel methods and deep learning approaches for regression are slightly overlooked in the ultrasonic non-destructive testing community. Furthermore, to the best of the author's knowledge, a sensitivity analysis study of machine learning based regression applied to Scattering matrix images has not been investigated in the literature.

The scattering matrix was previously used to characterise small slots machined using electrical discharge machining (EDM) [28] and ellipses [39] and satisfactory results were obtained for these idealised defects in low-noise scenarios. These approaches were based on a nearest-neighbour-search scheme and yielded a single characterisation result. However, the signal-to-noise ratio of the time-domain signals (and hence, the extracted scattering matrices) can become very low in practical cases if a defect is unfavourably oriented (*e.g.*, when only the crack tip signal is measurable). Since the actual characterisation result can potentially have large errors in such challenging cases, uncertainty quantification is a prominent part of any defect characterisation procedure. In this paper, we explore the use of Bayesian inference and calculate the posterior probability of different defect parameters given some experimental measurement. Moreover, for a better understanding of the limitations of the Bayesian inference and the achievable characterisation performance using the scattering matrix, we also implemented some popular machine learning algorithms including linear regression, Gaussian process regression as well as CNNs, which take the scattering matrix data as the input and give defect parameters as the output. Importantly, we investigate how the measurement noise will affect the inversion results for different approaches. The main purpose of this paper is to identify the strengths and weaknesses of both approaches and to provide a guideline on the selection of the suitable inversion approach for different measurement scenarios in practical applications, such as ultrasonic array inspection of surface-breaking cracks, porosity, and inclusions.

II. Description of the inversion problem

The scattering matrix describes the angular scattering behaviour of a defect and consists of the far-field scattering coefficients for different incident-scattering angle pairs. Considering the 2-D geometry in Fig. 1, the scattering matrix is defined as [28]:

$$\boldsymbol{s}(\theta_i, \theta_s, \omega) = \frac{a_s(\omega)}{a_i(\omega)} \sqrt{\frac{d}{\lambda}} \exp\left(-\frac{i\omega d}{c}\right). \tag{1}$$

In Eq. (1), θ_i, θ_s denote the incident and scattering angles, a_i, a_s are the amplitude of the plane incident wave and the scattered wave, d is the distance between the receiver and the scatterer, and c is the wave speed in the medium. Note that bold upper- and lower- case symbols indicate matrices and vectors in this paper, and a wavelength (λ) is used as a normalisation distance in Eq. (1). The experimental data used in this paper were obtained through direct contact measurements, and only longitudinal

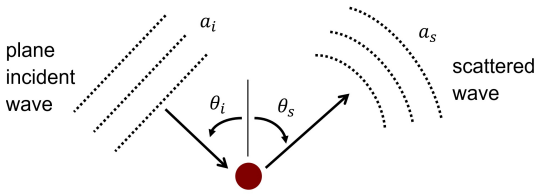

Fig. 1. Definition of the scattering matrix. The incident angle θ_i and scattering angle θ_s are defined with respect to the vertical direction, and are positive if measured clockwise.

TABLE I
SPECIFICATIONS OF THE ARRAY TRANSDUCERS USED FOR IMAGING (5 MHZ) AND SCATTERING MATRIX EXTRACTION (2.5 MHZ).

Number of elements	Element width (mm)	Element pitch (mm)	Element length (mm)	Central frequency (MHz)
64	0.53	0.63	10	5
64	0.35	0.5	15	2.5

waves are considered hereafter. As the size of a defect becomes comparable to the ultrasonic wavelength, imaging algorithms such as the TFM can no longer provide sufficient information for evaluation of the defect geometry. This is illustrated in Fig. 2, which shows the TFM imaging results of ideal horizontal cracks of sizes 4 mm, 2 mm, 1 mm, and 0.5 mm. A 5 MHz, 64 element array (see Table I) is used in simulation (the wavelength is 1.26 mm at the array centre frequency), and the cracks are located at a depth of 20 mm from the array centre. The FMC array data used to calculate the TFM images in Fig. 2 are obtained using a hybrid model [11] which combines the classic linear systems model of the wave propagation [40] and the defect scattering model (*i.e.*, the scattering matrix). Fig. 3 shows the scattering matrices of these cracks as a comparison. As shown in Figs. 2(a)-2(b), the two larger cracks can be readily sized from their TFM results. However, the defect indication has a larger dimension in z-axis for the results of the two smaller cracks in Figs. 2(c)-2(d), which can be mistakenly assumed as an indication of cracks with vertical orientations. On the contrary, the amplitude of the scattering matrix drops monotonically as the crack size decreases. Combined with a change in the shape of the scattering matrix, all the cracks are seen to be distinguishable using the scattering matrix. Hence, using the scattering matrix is an efficient approach to characterising defects smaller than 2λ, and image-based characterisation can be used if the defect size exceeds 2λ [11].

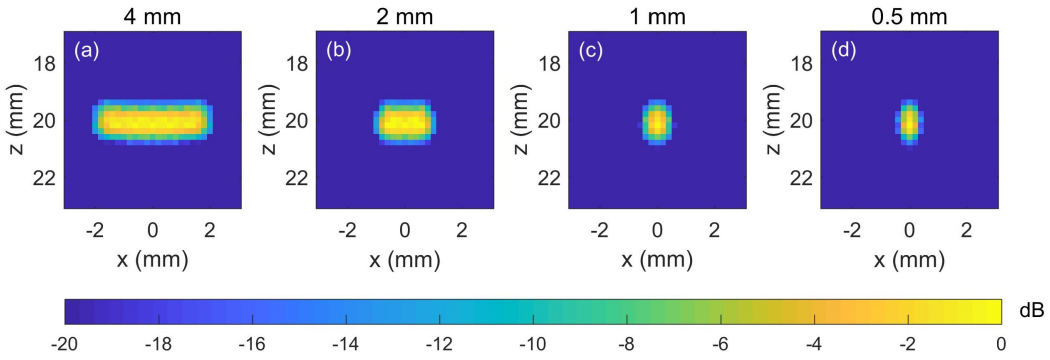

Fig. 2. TFM imaging results of horizontal cracks of sizes (a) 4 mm, (b) 2 mm, (c) 1 mm, and (d) 0.5 mm. A 5 MHz, 64 element linear array (see Table I) is used in simulation to generate the FMC array data.

The use of the scattering matrix for inversion is not limited to certain defect types or parameters. To illustrate this, we consider in this paper characterisation of small surface-breaking notches in an Aluminium test specimen [41]. The FMC data is measured from 8 EDM notches which have different sizes and orientation angles as specified in Table II (test configuration is same for all the notches and is shown in Fig. 4). This experimental configuration allows separation of the defect signal and backwall reflection in the time-domain, thus helps avoid the additional complexity caused by the need to suppress the strong backwall reflections when extracting the defect scattering matrix [42]. The scattering matrices are extracted from experimental FMC data using the sub-array imaging approach [11].

The scattering matrix of an ideal smooth surface-breaking crack can be obtained using a finite element modelling approach [43]. This model is based on an integral representation of the scattered wave field, and generation of the input plane wave and monitoring of the scattered wave are completed at nodes on two concentric surfaces that enclose the defect [43]. Hence, the

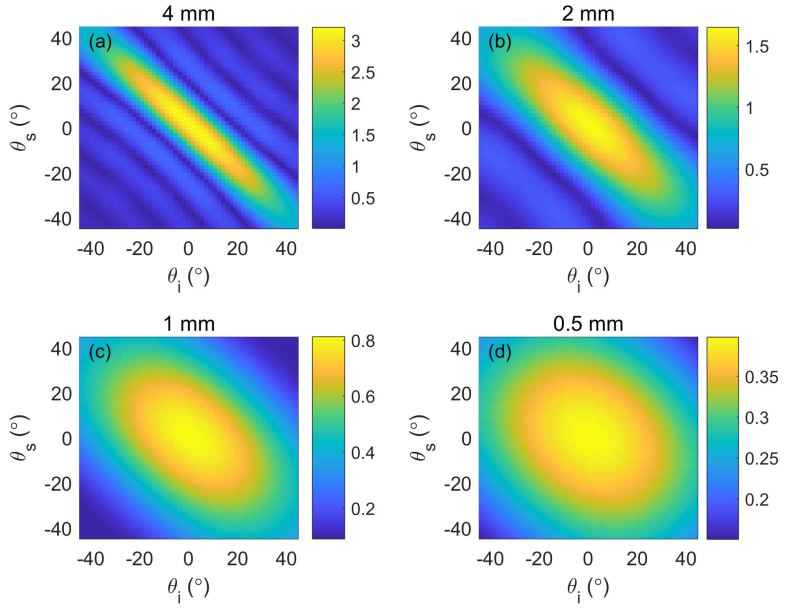

Fig. 3. Scattering matrices of horizontal cracks, where the crack sizes are: (a) 4 mm, (b) 2 mm, (c) 1 mm, and (d) 0.5 mm.

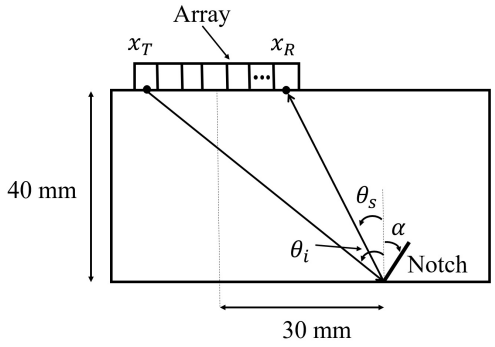

Fig. 4. Measurement configuration adopted in experiments for characterisation of the surface-breaking notches. A 2.5 MHz, 64 element array (see Table I) is used in experiments.

TABLE II
SIZES (WAVELENGTHS) AND ANGLES (DEGREES) OF THE EDM NOTCHES. WHEN THE FREQUENCY IS 2.5 MHZ, $\lambda = 2.5$ MM IN ALUMINIUM.

Notch	1	2	3	4	5	6	7	8
Size	0.80	0.83	0.92	1.13	1.20	1.24	1.39	1.70
Angle	0	15	30	45	0	15	30	45

TABLE III
RANGES AND SAMPLING INTERVALS OF THE DEFECT PARAMETERS FOR THE TRAINING AND TEST SETS.

Dataset	Size (wavelengths)		Angle (degrees)	
	Range	Interval	Range	Interval
Training	from 0.50 to 2.00	0.1	from -60 to 60	2
Test	from 0.55 to 1.95	0.1	from -55 to 55	10

spatial size of the modelling domain around the defect is small (*i.e.*, local to the defect) and it allows fast evaluation of the forward model. Scattering matrices used as the training and test examples are simulated by adopting this approach and more details about the training and test sets can be found in Table III.

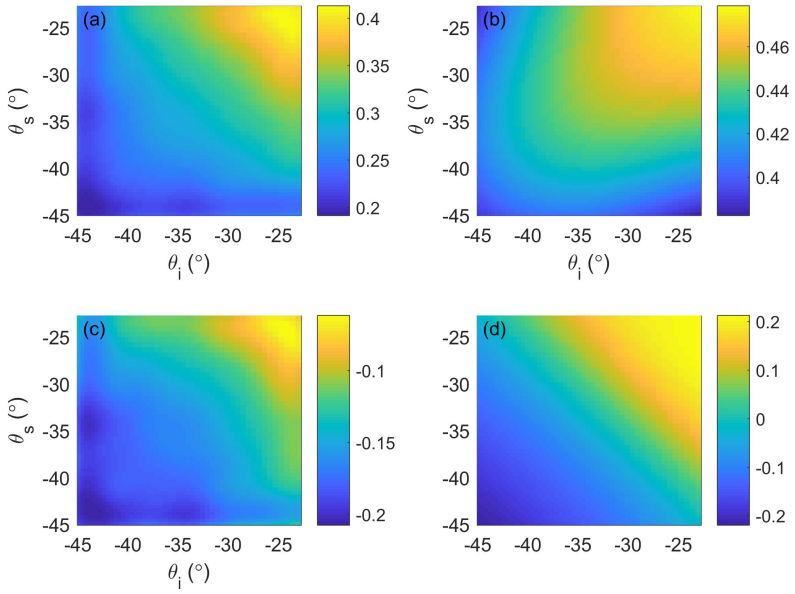

Fig. 5. (a) Experimentally measured scattering matrix of Notch 1, (b) scattering matrix of an ideal surface-breaking crack with the same size and angle as Notch 1, (c) experimental noise, and (d) a random noise realisation obtained from the noise model.

Measurement noise is an important challenge for the inversion problem. In this paper, we define noise as the difference between the measured scattering matrix and its idealised noise-free version (*i.e.*, those included in the training set). For example, Fig. 5(a) shows the scattering matrix of Notch 1 extracted from experimental FMC data. The scattering matrix of an ideal surface-breaking crack having the same size and angle as Notch 1 is shown in Fig. 5(b), and Fig. 5(c) is the experimental noise. It can be seen from Fig. 5(c) that the actual experimental noise is coherent (as random noise can be removed by simple averaging or filtering operations). In order to simulate multiple realisations of coherent noise for sensitivity analysis, a 2D Gaussian rough surface model (also termed the general coherent noise model in Ref. [41]) is adopted. The Gaussian rough surface noise model has been applied to different measurement scenarios (*e.g.*, characterisation of small machined notches and elliptical voids) for uncertainty quantification [44], and parameters of the noise model such as the RMS roughness and correlation lengths can be determined using a maximum-likelihood estimation approach [41]. In addition, as will be explained in Section III-A, the characterisation result (*i.e.*, the posterior probability of the defect parameter) can be calculated analytically based on the general rough surface noise assumption. Fig. 5(d) shows a random realisation of the simulated noise obtained by running the Gaussian rough surface model. The noise database $\boldsymbol{N}^{db} = [\boldsymbol{n}_1, \boldsymbol{n}_2, \ldots, \boldsymbol{n}_M]$ contains M =1000 such random noise realisations and is used to evaluate and compare robustness of the two inversion approaches considered in this paper. More details about the Gaussian rough surface model can be found in Ref. [41].

III. The Defect Characterisation Approaches

A. The Bayesian approach

In this approach, the inversion problem is formulated as calculating $P(\boldsymbol{p}|\boldsymbol{s}_n)$, *i.e.*, the conditional probability of the defect parameter $\boldsymbol{p}$ given the measurement of the scattering matrix $\boldsymbol{s}_n$. Using Bayes' theorem, we have [45]:

$$P(\boldsymbol{p}|\boldsymbol{s}_n) = \frac{P(\boldsymbol{s}_n|\boldsymbol{p})P(\boldsymbol{p})}{P(\boldsymbol{s}_n)}. \tag{2}$$

In the above equation, the subscript n refers to the scattering matrix containing noise, such that

$$\boldsymbol{s}_n = \boldsymbol{s}_p + \boldsymbol{n}, \tag{3}$$

where $\boldsymbol{s}_p$ is the scattering matrix of an ideal defect with parameter $\boldsymbol{p}$ and $\boldsymbol{n}$ represents noise [see for example, Fig. 5(d)]. Without *a priori* knowledge about the defect or measurement noise, it is reasonable to assume that the ratio of the prior distributions $P(\boldsymbol{p})$ and $P(\boldsymbol{s}_n)$ is a constant C [41]. If we further assume that the probability of noise $\boldsymbol{n}$ is independent of the defect parameter $\boldsymbol{p}$ (and hence, the scattering matrix $\boldsymbol{s}_p$), we can conclude from Eqs. (2)-(3) that

$$P(\boldsymbol{p}|\boldsymbol{s}_n) = CP(\boldsymbol{n}). \tag{4}$$

Eq.(4) provides a convenient way of calculating the defect characterisation result. Note that the noise vector $\boldsymbol{n}$ in the noise database follows a multivariate Gaussian distribution and its components become independent in principal-component space [41]. For the noise database $\boldsymbol{N}^{db}$ prepared in Section II, the principal component analysis (PCA) procedure can be performed in following two steps [46]:

Step 1. Calculate the covariance matrix as $\boldsymbol{N}_{cov} = (\boldsymbol{N}^{db} - \boldsymbol{N}_0)(\boldsymbol{N}^{db} - \boldsymbol{N}_0)^T/(M-1)$. $\boldsymbol{N}_0 = [\boldsymbol{n}_0, \boldsymbol{n}_0, \ldots, \boldsymbol{n}_0]$ and $\boldsymbol{n}_0$ is the mean noise vector of the noise database.

Step 2. Perform eigendecomposition of the covariance matrix as $\boldsymbol{N}_{cov} = \boldsymbol{V}\boldsymbol{D}\boldsymbol{V}^T$.

The defect characterisation result can then be obtained by calculating the noise $\boldsymbol{n}$ and its probability $P(\boldsymbol{n})$. Based on the result of the PCA process, $P(\boldsymbol{n})$ can be expressed as

$$P(\boldsymbol{n}) = P(\boldsymbol{n}^{pc}) = \frac{1}{(2\pi)^{N_s/2}|\boldsymbol{D}|^{1/2}} \exp\left(-\boldsymbol{n}^{pc}\boldsymbol{V}\boldsymbol{D}^{-1}\boldsymbol{V}^T\boldsymbol{n}^{pc}\right), \tag{5}$$

where

$$\boldsymbol{n}^{pc} = \boldsymbol{V}^T(\boldsymbol{s}_n - \boldsymbol{s}_p - \boldsymbol{n}_0), \tag{6}$$

represents the noise vector $\boldsymbol{n}$ in the principal-component space and N_s is the dimensionality of the noise vector $\boldsymbol{n}^{pc}$. In Section IV, we calculated the conditional probability $P(\boldsymbol{p}|\boldsymbol{s}_n)$ using Eqs. (4)-(5) for the defect parameter $\boldsymbol{p}$ that is evenly distributed in the 2D parameter space (*i.e.*, corresponding to the training points in Table III). The result of the Bayesian approach will then be presented in the form of probability maps.

B. Application of the machine learning approaches

1) Overview of machine-learning approaches: Let us consider a second approach for the defect characterisation task, which casts the problem in a supervised machine learning (ML) setting. The problem is set up in the following way: we employ the training and test databases described in Table III and train several machine learning algorithms on the training set to learn the mapping between the scattering matrices and the defect parameters (*i.e.*, size and angle). It should be noted that the trained regression models are then inverse models and can be used directly to obtain estimates of defect parameters from scattering matrices, unlike classical inversion schemes. The learned models are evaluated on the test set and the experimentally measured scattering matrices of machined notches.

A major difference between machine learning approaches and the Bayesian approach described above is that the machine learning models do not account for the existence of noise directly in their formulations. However, an approach for taking into account the influence of noise is developed and applied while characterizing the experimental scattering matrices of Notches 1-8 as will be explained below.

Three machine learning approaches are considered in this paper: linear regression (used as a baseline), a kernel model (Gaussian process regression) that uses a dimensionality reduction technique, and a deep convolutional neural network that implicitly learns a lower-dimensional manifold.

2) Generation of the training and test sets and dimensionality reduction: We define the training and test sets for the machine learning approaches as the collection of input-target pairs:

$$\begin{aligned} \boldsymbol{S}_T =& \{(\boldsymbol{x}_1, \boldsymbol{y}_1), \ldots, (\boldsymbol{x}_{N_T}, \boldsymbol{y}_{N_T})\} \equiv (\boldsymbol{X}_T \times \boldsymbol{Y}_T)^{N_T}, \\ & \text{where } T = \{tst, trn\}. \end{aligned} \tag{7}$$

In the above equation, the i-th couple $(\boldsymbol{x}_i, \boldsymbol{y}_i)$ represents the i-th input vector and the associated i-th target (or label) within $\boldsymbol{S}_{trn}$ or $\boldsymbol{S}_{tst}$ sets. Here we assume that $\boldsymbol{x}_i \in \mathbb{R}^{M\times 1}$ and $\boldsymbol{y}_i \in \mathbb{R}^{P\times 1}$, where M represents the number of the scattering coefficients within a scattering matrix and P is the number of parameters to be retrieved.

It can be seen from Table III that the training and test sets were generated with defect parameters on non-overlapping grids. The size of the training set was $N_{trn} = 976$ samples whereas the test set held $N_{tst} = 180$ samples. Note that the number of the scattering coefficients in a scattering matrix is equal to $M = 64^2 = 4096$ when using a 64 element array without the sub-array method. In order to remove such a large cardinality and mitigate the so-called curse of dimensionality issue [47], we apply PCA feature extraction on the scattering matrix data. Using PCA, we can significantly reduce the dimensionality of the input features by projecting the original data into principal-component space following the Steps 1 and 2 detailed in Section III-A.

3) Linear and kernel based models for regression: As a baseline, a linear regression (LR) model is used. Each sample in the scattering matrix database is considered as a vector (instead of a 2D image) by collapsing the rows, and the PCA is applied to reduce the dimensionality of the database. A linear model is then fitted using the extracted features and corresponding defect parameters.

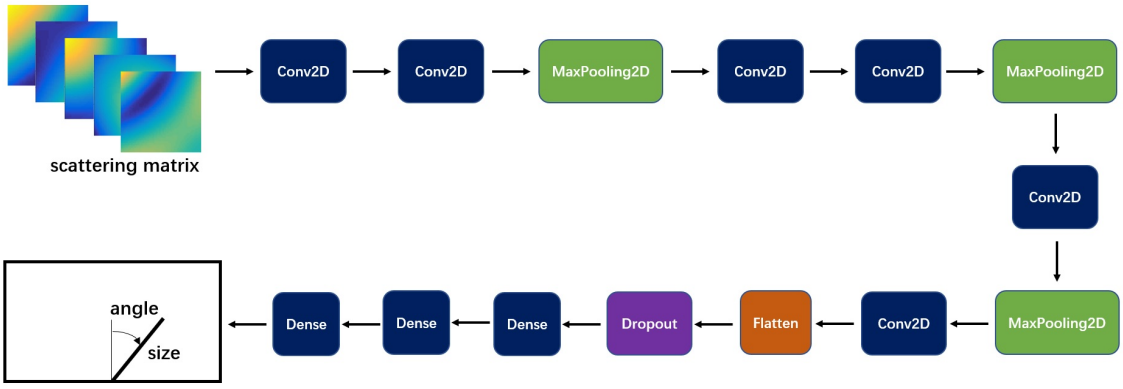

Fig. 6. Sketch of the SMInvNet architecture.

As a second model, a Gaussian process regression (GPR) [48] is applied to the scattering matrix database. Following Ref. [49], we start with the PCA-extracted features and fit a kriging predictor which yields an approximate solution $\hat{\mathbf{y}}$ of the inverse problem of finding the parameters giving rise to the observation $\boldsymbol{x}$ as a linear combination of the input vectors:

$$\hat{\mathbf{y}} = \sum_{i=1}^{N_{trn}} \lambda_i(\mathbf{x})\mathbf{y}_i, \tag{8}$$

with the weights $\lambda_i(\mathbf{x})$ computed in a stochastic framework. Each parameter $\mathbf{y}_i$ is modeled as a Gaussian random process, defined by its mean and covariance functions.

The coefficients $\lambda_i(\mathbf{x})$ are chosen according to the following linear system of equations:

$$\begin{bmatrix} k(||\mathbf{x_1}-\mathbf{x_1}||) & \cdots & k(||\mathbf{x_1}-\mathbf{x_{N_{trn}}}||) \\ \vdots & \ddots & \vdots \\ k(||\mathbf{x_{N_{trn}}}-\mathbf{x_1}||) & \cdots & k(||\mathbf{x_{N_{trn}}}-\mathbf{x_{N_{trn}}}||) \end{bmatrix} \begin{bmatrix} \lambda_1(\mathbf{x}) \\ \vdots \\ \lambda_n(\mathbf{x}) \end{bmatrix} = \begin{bmatrix} k(||(\mathbf{x}-\mathbf{x_1})|| \\ \vdots \\ k(||(\mathbf{x}-\mathbf{x_{N_{trn}}})|| \end{bmatrix}. \tag{9}$$

The covariance function $k(\cdot)$ is unknown and one has to predict it using the training samples. In this work, we have used the rational quadratic covariance model.

4) Convolutional Neural Networks for regression: Since the seminal 2012 paper on image classification [50], deep convolutional neural networks (CNN) have shown that they are well adapted to all sorts of image-related tasks. Building upon the previous work [51], we propose to use a CNN network architecture specifically tailored on the scattering matrix data targeting inversion (regression) tasks. In the following, we refer to this architecture as "SMInvNet". SMInvNet is composed of two CNN stages made of two blocks. The first two blocks contain two convolutional layers and a max-pooling layer. For each block, the convolutional layer and the pooling layer has 32 and 64 feature map channels. The third block composed by a CNN layer and a max-pooling layer having size equal to 128 feature map channels, was concatenated to another CNN layer made by 128 feature map channels. The fully connected part is based on a dropout layer, with drop-out rate equal to 0.4, and two fully-connected layers made of 2048 neurons each. Rectified linear unit activation functions have been employed for all layers and Adam optimizer with learning rate equal to 1e-4 was employed to optimize the network weights and biases. The total number of trainable parameters was approximately equal to 13.8 million. The sketch of the architecture is provided in Fig. 6.

The SMInvNet takes the 2D scattering matrix as its input data. The convolutional layers extract features by convolving the input data with learnable kernels. An output convolutional feature I^{l+1} at layer $l+1$ is computed from I^l of the previous layer using the relationship $I^{l+1} = \mathcal{C}(I^l)$. More specifically, on a pixel-by-pixel basis we have

$$I^{l+1}_{m,n} = \sum_a \sum_b w^{l+1}_{a,b} \eta(I^l_{m-a,n-b}) + b^{l+1}_{m,n}, \tag{10}$$

where m and n are the pixel coordinates of the image, $w^{l+1}_{a,b}$ are the weights, η is the activation function and $b^{l+1}_{m,n}$ are the biases. The weights and biases are to be learned on the data while the activation function is set in advance (here, we use a

rectified linear unit function). The backpropagation algorithm and ADAM minimization algorithm [52] are used to adjust the weights and biases by minimizing the loss function, which is defined here as the mean absolute error.

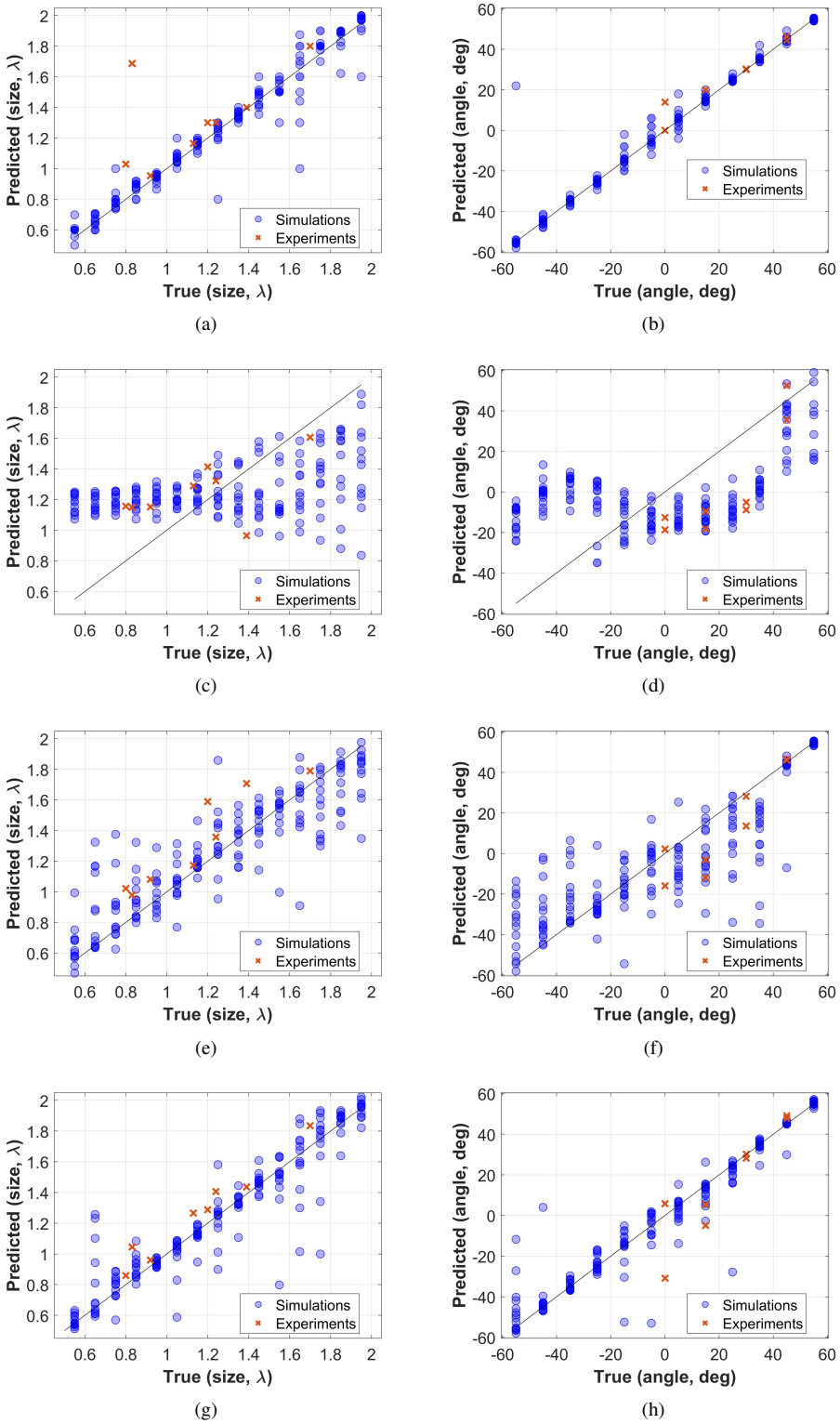

Fig. 7. Test set results of different inversion approaches in terms of defect size (left column) and angle (right column), where (a)-(b) Bayesian, (c)-(d) PCA-LR, (e)-(f) PCA-PGR, and (g)-(h) SMInvNet are used, respectively.

TABLE IV
NUMBER OF OUTLIERS (SIZING ERRORS GREATER THAN 0.2λ AND/OR ANGLE ERRORS GREATER THAN 20°) OF DIFFERENT INVERSION APPROACHES OBTAINED ON THE TEST SET.

Parameter	Bayesian	PCA-LR	PCA-GPR	SMInvNet
size	11	130	43	21
angle	1	115	46	7

IV. RESULTS

A. Results on the test set

In this section, we present the results obtained on the test set. Figs. 7(a)-7(b) show the size and angle results of the Bayesian approach, where the predicted parameter values are plotted against the true values. When implementing the Bayesian approach for the test samples, the noise model introduced in Section II was used for calculating the probability distribution of the defect parameter. The set of defect parameters that gives the maximum probability is then plotted as circles (for simulated noise-free data) and crosses (for experimental data).

An important difference between the Bayesian and machine learning approaches is that the noise model is not explicitly used in the machine learning approaches for defect characterisation. Based on the training data, we have tuned the LR and the GPR models by employing a 5-fold cross validation (CV) procedure. The CV has been employed to optimise the number of PCA components for the LR and GPR models, as well as the model hyper-parameters of the GPR covariance matrix. The number of principal components selected was equal to four, and this corresponds to 99% of the explained variance.

Figs. 7(c)-7(f) show the results obtained with the LR and GPR models. The baseline linear regression model performs poorly in this context and shows many severe outliers (sizing errors greater than 0.2λ and/or angle errors greater than 20°, see Table IV), with high variance and bias in predictions. This implies that the relationship between the input (the scattering matrix) and the output (defect size and angle) is non-linear, which necessitates the use of more sophisticated machine learning algorithms. The GPR model handles defect size estimation better, even though a considerable variance is found in the predicted data (see Fig. 7(e)). In addition, high bias and variance have been observed for the angle results (see Fig. 7(f)). From the results of the GPR model, one can infer that it generalises to experimental data as well as it does on the synthetic simulation data.

TABLE V
ERROR METRICS [SIZE (λ) AND ANGLE (DEGREES)] FOR PERFORMANCE EVALUATION OF THE STUDIED INVERSION ALGORITHMS: BAYESIAN, LINEAR REGRESSION (LR), GAUSSIAN PROCESS REGRESSION (GPR) AND DEEP CONVOLUTIONAL NEURAL NETWORK (SMINVNET).

Metric	Bayesian		PCA-LR		PCA-GPR		SMInvNet	
	size	angle	size	angle	size	angle	size	angle
MAE	0.06	2.10	0.33	25.18	0.14	12.75	0.08	4.88
RMSE	0.09	6.39	0.39	28.79	0.20	18.61	0.12	9.54
R2	0.95	0.97	0.16	0.29	0.77	0.71	0.92	0.92

To quantify the performance of different inversion approaches, we use standard metrics on the predictions, namely mean absolute error (MAE), root mean square error (RMSE) as well as R^2 coefficient of determination (see Table V). In contrast to the LR and GPR models above where the feature extraction was performed via PCA, SMInvNet learns its own feature descriptors without the need for explicit dimensionality reduction. As can be seen in Figs. 7(g)-7(h), the SMInvNet provides notably better predictions than the LR and GPR models. Indeed, both bias and variance in the predicted results remain low. Moreover,on the same plots, one can notice that SMInvNet is able to generalize well on real experimental data.

Overall, the Bayesian approach is seen to have achieved the best characterisation performance on the simulated data. The SMInvNet model gives comparable characterisation accuracy for most test samples, but it produced increased number of outliers as can be found in Table IV. It is suggested that the use of (the optimised) noise model has contributed to the high accuracy of the Bayesian approach. Interestingly, the overall sizing performance is seen to be poorer for larger defects. The main contribution to this outcome comes from unfavorably oriented large cracks. Because of the small amplitude of the tip diffracted signal, characterisation of these unfavourably oriented cracks is more challenging and their sizes are more likely to be underestimated. For the smallest (0.55λ) cracks in the test set, the sizing results given by the SMInvNet model (mean:0.564λ, standard deviation: 0.038λ) are found to be more accurate than those of the Bayesian approach (mean:0.597λ, standard deviation: 0.044λ).

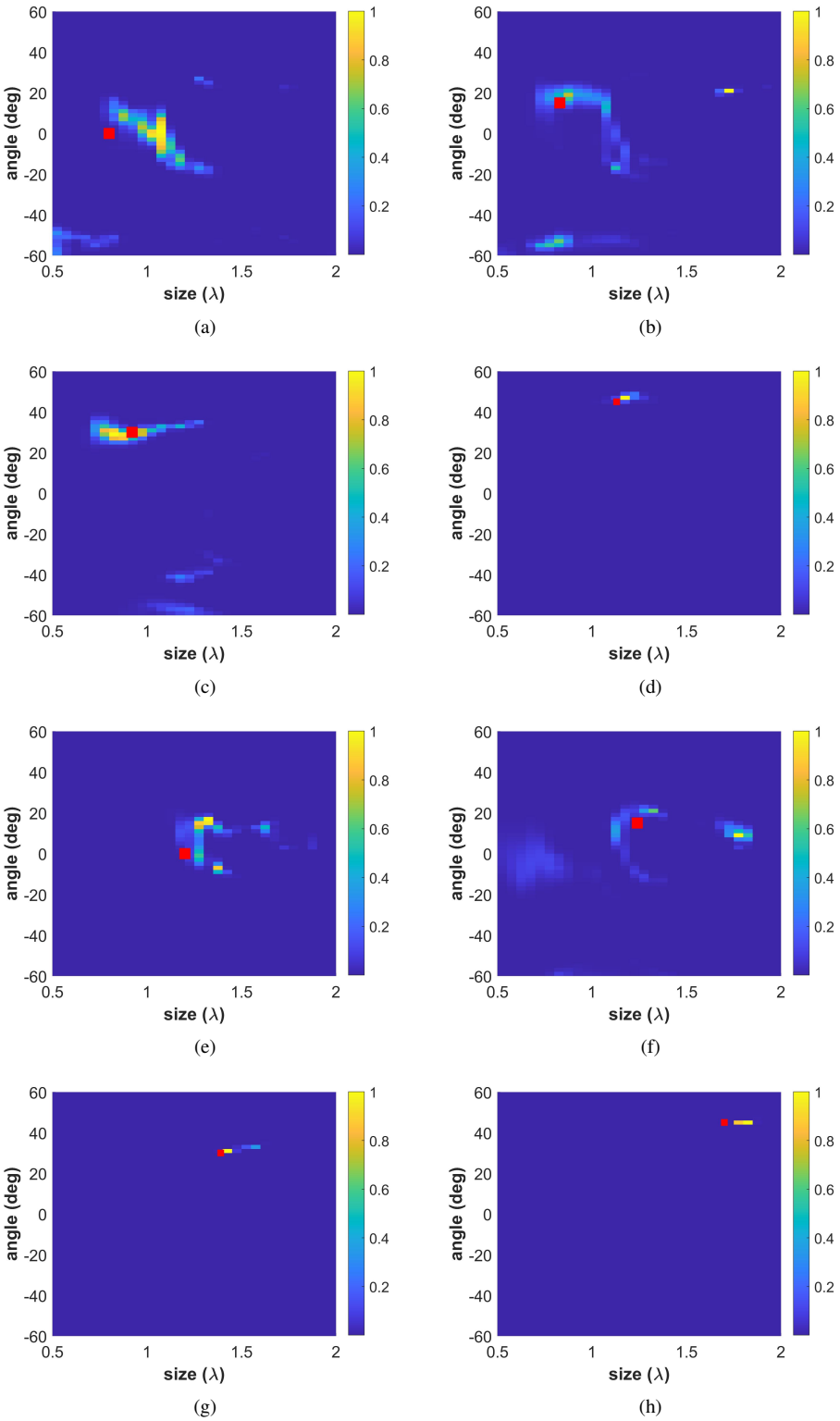

Fig. 8. Uncertainty analysis for the experimental measurements of machined notches (see Table II) using the Bayesian inversion approach. The colour bars show the normalised probability.

B. Uncertainty analysis

Figs. 8(a)-8(h) are the characterisation results of Notches 1-8 in the test specimen, obtained using the Bayesian inversion approach. The red squares in these results correspond to the true defect parameters, and they are in general close to the maximum probability points. Although the maximum probability points give large errors for Notches 2 and 6, the true parameter points

are seen to be near the secondary peaks in Figs. 8(b) and 8(f), which demonstrates the robustness of the Bayesian approach.

As explained in the previous section, the ML model outputs a single prediction of defect size and angle for each test scattering matrix. In the context of defect characterisation, it is however of paramount interest to evaluate the uncertainty associated with the inversion procedure. Here we propose a methodology to empirically evaluate the characterisation uncertainty caused by the measurement noise for the SMInvNet model. This approach is similar in spirit to the one in Ref. [26].

To add uncertainty estimates to our analysis, we use the noise database $\boldsymbol{N}^{db}$ prepared in Section II. This database allows us to prepare experimental scattering matrices with additive noise. The noisy scattering matrices are obtained by adding one of the noise realisations to the noise-free data as follows:

$$\exists k, \boldsymbol{x}_{noisy} = \boldsymbol{x}_i + \boldsymbol{n}_k^{db}. \tag{11}$$

For sake of brevity and due to the higher accuracy shown by the SMInvNet model, we focus only on the evaluation of this model. Each noisy scattering matrix yields a single characterisation result (*i.e.*, a point in the two-dimensional defect parameter space), and Fig. 9 shows the 2D histogram of all 1000 characterisation results (bin centres of the histogram are the same as the grid points of the probability map in Fig. 8). As can be seen in Fig. 9, the probability distribution is quite peaked for Notches 4, 7 and 8 and thus implies high confidence. For Notches 1 and 3, the probability distribution is either very spread out or bi-modal, implying low confidence in the prediction. Notch 2 seems to be in-between since it is peaked but spreads out much into the defect parameter space.

The characterisation results shown in Figs. 8 and 9 for the Bayesian and SMInvNet model are compared in Table VI, where the characterisation performance is evaluated qualitatively based on the bias and variance of the results. It can be concluded from Figs. 8-9 and Table VI that the characterisation results of both approaches are indeed very similar for favourably oriented defects (Notches 4, 7, and 8). The Bayesian approach has produced more accurate results with lower uncertainty for Notches 1 and 5. The SMInvNet model is seen to give a higher variance in most cases, but it avoided the large sizing errors of the Bayesian approach for Notches 2 and 6.

TABLE VI
COMPARISON OF THE CHARACTERISATION RESULTS OF THE BAYESIAN AND SMINVNET MODELS FOR THE EXPERIMENTAL MEASUREMENTS OF MACHINED NOTCHES.

Notch	Bayesian	SMInvNet
1	High bias / small variance	High bias / high variance
2	High bias / high variance	High bias / high variance
3	Low bias / high variance	Low bias / high variance
4	Low bias / low variance	Low bias / low variance
5	Low bias / low variance	Low bias / high variance
6	High bias / high variance	Low bias / low variance
7	Low bias / low variance	Low bias / low variance
8	Low bias / low variance	Low bias / low variance

V. DISCUSSIONS AND CONCLUSIONS

With the development of ultrasonic array transducers and data acquisition technology, the NDT industry now has access to larger amount of measurement data than ever before. Therefore, the selection of appropriate data processing technique (among many options that are available) has become a key issue for tasks such as defect characterisation. In this paper, we conducted a comparative study of the characterisation performance of the Bayesian inversion and machine learning approaches. The studied problem is the characterisation of surface-breaking cracks. The training and test sets consist of simulation data that cover the size range between 0.5λ and 2λ, and the angle range between -60° and 60°. In addition, experimental data measured from 8 machined notches are also used for testing. Among the three machine learning approaches considered in this paper, the SMInvNet (a convolutional neural network used for regression) achieves the best characterisation performance on the test set. The Bayesian inversion approach gives similar results for most test samples, and it also reduces the number of outliers compared to the SMInvNet model (number of large size and angle errors reduced by 5.3% and 3.2%, respectively). The characterisation uncertainty of both approaches is seen to be similar for favorably oriented defects. For unfavourably oriented defects, there is no clear "winner" and the performance of both approaches varied with different test samples. Overall, the results of the Bayesian approach exhibited higher bias while the SMInvNet model yielded higher variance, and hence, one faces the bias-variance tradeoff when choosing the appropriate characterisation approach for unfavourably oriented defects.

It is also interesting to compare the two approaches across other dimensions. Firstly, the Bayesian inversion approach is a specialized method that was developed specifically to address the defect characterisation problem based on the extraction of the scattering matrix, while the SMInvNet neural network reuses an architecture that could be applied to any type of images. Hence,

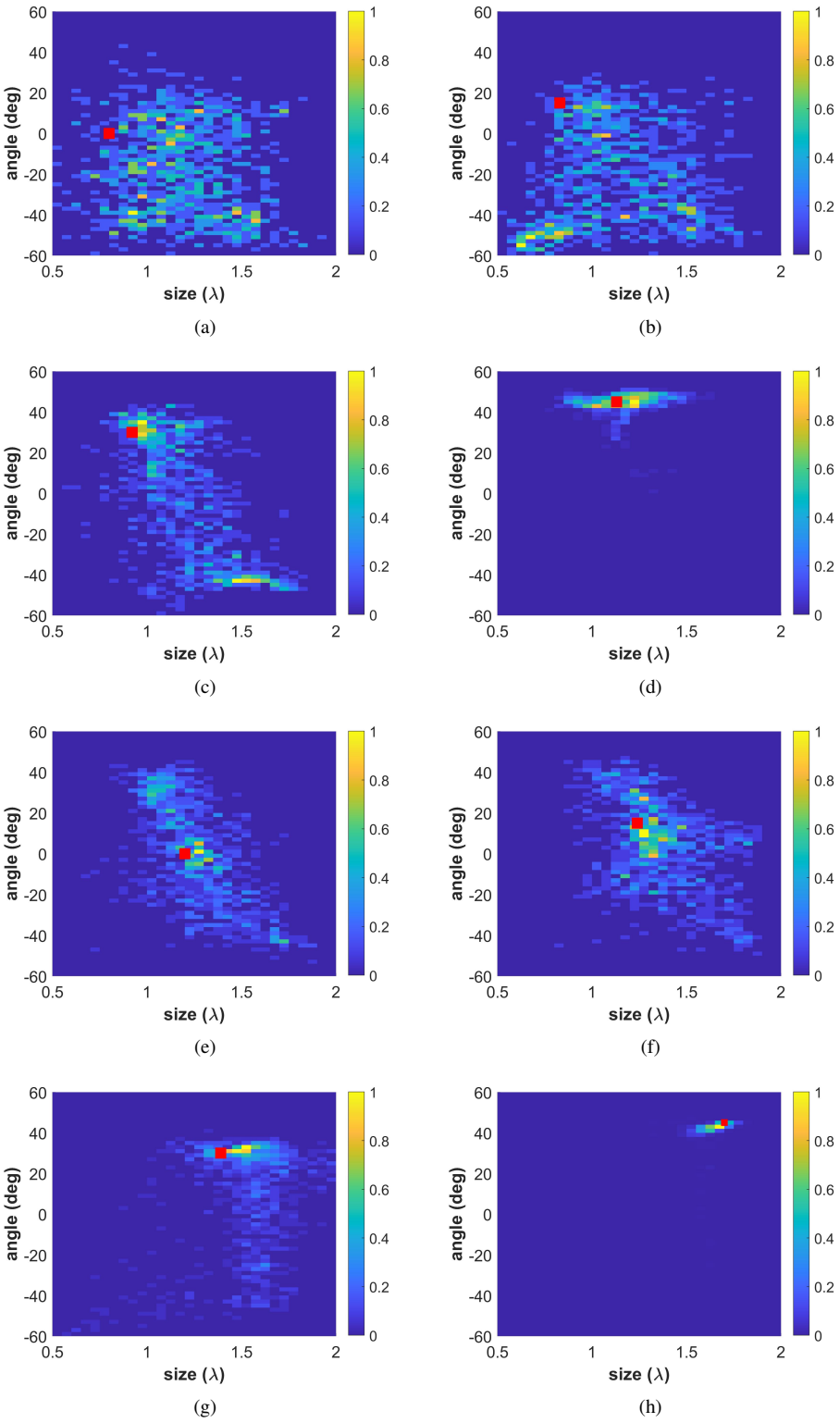

Fig. 9. Uncertainty analysis for the experimental measurements of machined notches (see Table II) using the SMInvNet model. The colour bars show the normalised probability.

depending on the background of the user, one may be more readily usable than the other. In particular, the acoustic domain knowledge is necessary for using the correct noise parameters in the Bayesian inversion method (in our case, 4 parameters are needed), which rely on the understanding of the underlying scattering matrix noise distribution. It is also desirable to develop a comprehensive noise model which takes into account all possible sources of noise for a given test configuration, and the

characterisation result is expected to improve by adopting more accurate noise models. That being said, some sort of domain knowledge is also necessary to design the SMInvNet network. Here the machine-learning domain knowledge is required to choose the right architecture such as number of layers, number of of filters, and the size of pooling layers.

Another dimension of interest to the end user is how different approaches deal with the uncertainty associated to the inversion problem. The Bayesian inversion approach naturally maps the confidence in the defect parameter to the probability. This is not the case for the SMInvNet model, and additional steps were adopted to allow for an uncertainty analysis. As we have shown in this paper, these two *different* paths led to comparable results.

A closely related question is how to interpret the uncertainty results. The Bayesian inversion method provides an explicit interpretation of the different terms that make up the probability, while the SMInvNet neural network is a "black box" with no straightforward way of interpreting the different model components. There are ongoing works which aim at developing tools that facilitate better interpretation of the internal structure of neural networks such as the one used in this paper. Hence, it is reasonable to expect that the "black box" issue can be resolved in the future by making use of the technology advances in the field of data science.

Both approaches are compatible with real-time use, since the learning (or fitting) step can be accomplished offline. The Bayesian approach would be restricted to problems of small cardinality since it is based on a grid-like evaluation of the posterior probability, while the neural network is not explicitly limited by this aspect of the inversion problem. This is a consequence of the curse of dimensionality when applied to grid methods.

At last, we note that turning to problems with a larger number of unknowns would affect the two approaches differently: the Bayesian model and its noise part could be fitted based on the summary statistics of the scattering matrix database, while the neural network would need to find a different path through the high-dimensional space in which it is trained using backpropagation.

An interesting research question based on this work would be asking how to combine the different types of imaging methods that use ultrasonic data coming from FMC data acquisition to enhance defect sizing performance. For instance, reconstruction algorithms such as TFM and plane wave imaging can help characterize wavelength-sized scatterers while Scattering Matrix images can help identify sub-wavelength reflectors. Toward this end, the approach proposed by [31] could probably be investigated.

REFERENCES

[1] T. Kundu, *Ultrasonic Nondestructive Evaluation: Engineering and Biological Material Characterization*. Boca Raton, FL: CRC Press, 2004.

[2] S. J. Song, H. J. Shin, and Y. H. Jang, "Development of an ultrasonic phased array system for nondestructive tests of nuclear power plant components," *Nucl. Eng. Design*, vol. 214, no. 1-2, pp. 151–161, 2002.

[3] N. Brierley, T. Tippetts, and P. Cawley, "Data fusion for automated non-destructive inspection," *Proc. R. Soc. A*, vol. 470, no. 2167, p. 20140167, 2014.

[4] J. Blitz and G. Simpson, *Ultrasonic methods of non-destructive testing*. London, UK: Chapman & Hall, 1996.

[5] B. W. Drinkwater and P. D. Wilcox, "Ultrasonic arrays for non-destructive evaluation: A review," *NDT E Int.*, vol. 39, no. 7, pp. 525–541, 2006.

[6] C. Holmes, B. W. Drinkwater, and P. D. Wilcox, "Post-processing of the full matrix of ultrasonic transmit-receive array data for nondestructive evaluation," *NDT E Int.*, vol. 38, no. 8, pp. 701–711, 2005.

[7] M. Sutcliffe, P. Charlton, and M. Weston, "Multiple virtual source aperture imaging for non-destructive testing," *Insight*, vol. 56, no. 2, pp. 75–81, 2014.

[8] G. Montaldo, M. Tanter, J. Bercoff, N. Benech, and M. Fink, "Coherent plane-wave compounding for very high frame rate ultrasonography and transient elastography," *IEEE Trans. Ultrason. Ferroelectr. Freq. Control*, vol. 56, no. 3, pp. 489–506, 2009.

[9] L. Le Jeune, S. Robert, E. L. Villaverde, and C. Prada, "Plane wave imaging for ultrasonic non-destructive testing: Generalization to multimodal imaging," *Ultrasonics*, vol. 64, pp. 128–138, 2016.

[10] K. Kimoto, S. Ueno, and S. Hirose, "Image-based sizing of surface-breaking cracks by SH-wave array ultrasonic testing," *Ultrasonics*, vol. 45, no. 1–4, pp. 152–164, 2006.

[11] J. Zhang, B. W. Drinkwater, and P. D. Wilcox, "The use of ultrasonic arrays to characterize crack-like defects," *J. Nondestruct. Eval.*, vol. 29, no. 4, pp. 222–232, 2010.

[12] J. Camacho, D. Atehortua, J. F. Cruza, J. Brizuela, and J. Ealo, "Ultrasonic crack evaluation by phase coherence processing and TFM and its application to online monitoring in fatigue tests," *NDT E Int.*, vol. 93, pp. 164–174, 2018.

[13] B. Shakibi, F. Honarvar, M. D. Moles, J. Caldwell, and A. N. Sinclair, "Resolution enhancement of ultrasonic defect signals for crack sizing," *NDT E Int.*, vol. 52, pp. 37–50, 2012.

[14] M. Li, X. Li, C. Gao, and Y. Song, "Acoustic microscopy signal processing method for detecting near-surface defects in metal materials," *NDT E Int.*, vol. 103, pp. 130–144, 2019.

[15] S. A. Mosey, P. C. Charlton, and I. Wells, "Resolution enhancement of ultrasonic B-mode images," *Insight*, vol. 55, no. 2, pp. 78–83, 2013.

[16] L. Merabet, S. Robert, and C. Prada, "2-D and 3-D reconstruction algorithms in the Fourier domain for plane-wave imaging in nondestructive testing," *IEEE Trans. Ultrason. Ferroelectr. Freq. Control*, vol. 66, no. 4, pp. 772–788, 2019.

[17] E. A. Marengo, F. K. Gruber, and F. Simonetti, "Time-reversal MUSIC imaging of extended targets," *IEEE Trans. Image Process.*, vol. 16, no. 8, pp. 1967–1984, 2007.

[18] A. Kirsch, "Characterization of the shape of a scattering obstacle using the spectral data of the far field operator," *Inverse Probl.*, vol. 14, no. 6, pp. 1489–1512, 1998.

[19] J. B. Elliott, M. J. S. Lowe, P. Huthwaite, R. Phillips, and D. J. Duxbury, "Sizing subwavelength defects with ultrasonic imagery: An assessment of super-resolution imaging on simulated rough defects," *IEEE Trans. Ultrason. Ferroelectr. Freq. Control*, vol. 66, no. 10, pp. 1634–1648, 2019.

[20] C. Fan, M. Caleap, M. Pan, and B. W. Drinkwater, "A comparison between ultrasonic array beamforming and super resolution imaging algorithms for non-destructive evaluation," *Ultrasonics*, vol. 54, no. 7, pp. 1842–1850, 2014.

[21] K. M. M. Tant, A. J. Mulholland, and A. Gachagan, "A model-based approach to crack sizing with ultrasonic arrays," *IEEE Trans. Ultrason. Ferroelectr. Freq. Control*, vol. 62, no. 5, pp. 915–926, 2015.

[22] X. Li, N. Sun, Y. Song, and S. Zhang, "Sizing small crack-like flaws through non-ideal part surface using ultrasonic measurement model," *Res. Nondestruct. Eval.*, vol. 31, no. 3, pp. 147–163, 2020.

[23] L. Moreau, A. J. Hunter, A. Velichko, and P. D. Wilcox, "3-D reconstruction of sub-wavelength scatterers from the measurement of scattered fields in elastic waveguides," *IEEE Trans. Ultrason. Ferroelectr. Freq. Control*, vol. 61, no. 11, pp. 1864–1879, 2014.

[24] M. Brigante, "Numerical algorithm for defect reconstruction in elastic media with a circular ultrasonic scanning," *Eng. Anal. Bound. Elem.*, vol. 37, no. 3, pp. 551–557, 2013.

[25] R. Miorelli, X. Artusi, A. B. Abdessalem, and C. Reboud, "Database generation and exploitation for efficient and intensive simulation studies," *AIP Conf. Proc.*, vol. 1706, no. 1, p. 180002, 2016.

[26] R. Miorelli, F. Le Bourdais, and X. Artusi, "Assessing performance of flaw characterization methods through uncertainty propagation," *AIP Conf. Proc.*, vol. 1949, no. 1, p. 170001, 2018.

[27] M. J. Bianco, P. Gerstoft, J. Traer, E. Ozanich, M. A. Roch, S. Gannot, and C. A. Deledalle, "Machine learning in acoustics: Theory and applications," *J. Acoust. Soc. Am.*, vol. 146, no. 5, pp. 3590–3628, 2019.

[28] L. Bai, A. Velichko, and B. W. Drinkwater, "Characterization of defects using ultrasonic arrays: A dynamic classifier approach," *IEEE Trans. Ultrason. Ferroelectr. Freq. Control*, vol. 62, no. 12, pp. 2146–2160, 2015.

[29] M. Salucci, N. Anselmi, G. Oliveri, P. Calmon, R. Miorelli, C. Reboud, and A. Massa, "Real-time NDT-NDE through an innovative adaptive partial least squares SVR inversion approach," *IEEE Trans. Geosci. Remote Sens.*, vol. 54, no. 11, pp. 6818–6832, 2016.

[30] S. Ahmed, C. Reboud, P.-E. Lhuillier, P. Calmon, and R. Miorelli, "An adaptive sampling strategy for quasi real time crack characterization on eddy current testing signals," *NDT & E International*, vol. 103, pp. 154–165, 2019.

[31] R. J. Pyle and R. L. T. Bevan and R. R. Hughes and R. K. Rachev and A. Ait Si Ali and P. D. Wilcox, "Deep learning for ultrasonic crack characterization in NDE," *IEEE Trans. Ultrason. Ferroelectr. Freq. Control*, 2020, early access.

[32] J. O'Leary and K. Sawlani and A. Mesbah, "Deep learning for classification of the chemical composition of particle defects on semiconductor wafers," *IEEE Trans. Semicond. Manuf*, vol. 33, no. 1, pp. 72–85, 2020.

[33] Y. J. Cha and W. Choi and O. Büyüköztürk, "Deep learning-based crack damage detection using convolutional neural networks," *Comput.-Aided Civ. Infrastruct. Eng.*, vol. 32, no. 5, pp. 361–378, 2017.

[34] H. Song and Y. Yang, "Super-resolution visualization of subwavelength defects via deep learning-enhanced ultrasonic beamforming: A proof-of-principle study," *NDT E Int.*, vol. 116, p. 102344, 2020.

[35] D. Zhang and K. Song and Q. Wang and Y. He and X. Wen and Y. Yan, "Two deep learning networks for rail surface defect inspection of limited samples with line-level label," *IEEE Trans. Ind. Informat.*, 2020, early access.

[36] M. Cacciola, S. Calcagno, F. C. Morabito, and M. Versaci, "Computational intelligence aspects for defect classification in aeronautic composites by using ultrasonic pulses," *IEEE Trans. Ultrason. Ferroelectr. Freq. Control*, vol. 55, no. 4, pp. 870–878, 2008.

[37] N. Laroche, S. Bourguignon, E. Carcreff, J. Idier, and A. Duclos, "An inverse approach for ultrasonic imaging from full matrix capture data. Application to resolution enhancement in NDT," *IEEE Trans. Ultrason. Ferroelectr. Freq. Control*, vol. 67, no. 9, pp. 1877–1887, 2020.

[38] R. Miorelli, A. Kulakovskyi, B. Chapuis, O. D'Almeida, and O. Mesnil, "Supervised learning strategy for classification and regression tasks applied to aeronautical structural health monitoring problems," *Ultrasonics*, vol. 113, p. 106372, 2021. [Online]. Available: https://www.sciencedirect.com/science/article/pii/S0041624X21000184

[39] L. Bai, A. Velichko, and B. W. Drinkwater, "Ultrasonic characterization of crack-like defects using scattering matrix similarity metrics," *IEEE Trans. Ultrason. Ferroelectr. Freq. Control*, vol. 62, no. 3, pp. 545–559, 2015.

[40] L. W. Schmerr, *Fundamentals of Ultrasonic Nondestructive Evaluation-A Modeling Approach*. New York, NY: Prenum Press, 1998.

[41] A. Velichko, L. Bai, and B. W. Drinkwater, "Ultrasonic defect characterization using parametric-manifold mapping," *Proc. R. Soc. A*, vol. 473, no. 2202, p. 20170056, 2017.

[42] J. Zhang, P. Yu, and T. Gang, "Measurement of the ultrasonic scattering matrices of near surface defects using ultrasonic arrays," *Nondestruct. Test. Eva.*, vol. 31, no. 4, pp. 303–318, 2016.

[43] A. Velichko and P. D. Wilcox, "A generalized approach for efficient finite element modelling of elastodynamic scattering in two and three dimensions," *J. Acoust. Soc. Am.*, vol. 128, no. 3, pp. 1004–1014, 2010.

[44] L. Bai and A. Velichko and A. T. Clare and P. Dryburgh and D. Pieris and B. W. Drinkwater, "The effect of distortion models on characterisation of real defects using ultrasonic arrays," *NDT E Int.*, vol. 113, p. 102263, 2020.

[45] T. Hastie, R. Tibshirani, and J. Friedman, *The elements of statistical learning*, 2nd ed. New York, NY: Springer-Verlag, 2009.

[46] I. T. Jolliffe, *Principal component analysis*, 2nd ed. New York, NY: Springer-Verlag, 2002.

[47] R. E. Bellman, *Adaptive Control Processes: A Guided Tour*. Princeton, NJ: Princeton Univ. Press, 1961.

[48] S. Theodoridis, *Machine Learning: A Bayesian and Optimization Perspective*. Academic press, 2015.

[49] S. Bilicz, M. Lambert, S. Gyimothy, and J. Pavo, "Solution of inverse problems in nondestructive testing by a kriging-based surrogate model," *IEEE Transactions on Magnetics*, vol. 48, no. 2, pp. 495–498, 2012.

[50] A. Krizhevsky, I. Sutskever, and G. E. Hinton, "Imagenet classification with deep convolutional neural networks," in *Advances in Neural Information Processing Systems*, 2012, pp. 1097–1105.

[51] A. Kulakovskyi, R. Miorelli, O. Mesnil, B. Chapuis, and O. D'Almeida, "Convolutional neural network for automated diagnostic from guided wave imaging in a structural health monitoring context," *Review of Progress in Quantitative Nondestructive Evaluation*, 2019.

[52] D. P. Kingma and J. Ba, "Adam: A method for stochastic optimization," *ArXiv Prepr. ArXiv1412.6980*, 2014. [Online]. Available: http://arxiv.org/abs/1412.6980